IOPscience iopscience.iop.org

Home Search Collections Journals About Contact us My IOPscience

MEASUREMENTS OF RAPID DENSITY FLUCTUATIONS IN THE SOLAR WIND

This article has been downloaded from IOPscience. Please scroll down to see the full text article.

2010 ApJ 711 322

(http://iopscience.iop.org/0004-637X/711/1/322)

The Table of Contents and more related content is available

Download details:
IP Address: 128.32.147.236
The article was downloaded on 15/03/2010 at 22:53

Please note that terms and conditions apply.

The Astrophysical Journal, 711:322–327, 2010 March 1 doi:10.1088/0004-637X/711/1/322
© 2010. The American Astronomical Society. All rights reserved. Printed in the U.S.A.

MEASUREMENTS OF RAPID DENSITY FLUCTUATIONS IN THE SOLAR WIND

D. M. Malaspina[1], P. J. Kellogg[2], S. D. Bale[3], and R. E. Ergun[1,4]
[1] Laboratory for Atmospheric and Space Physics, University of Colorado, Boulder, CO 80303, USA; David.Malaspina@colorado.edu
[2] School of Physics and Astronomy, University of Minnesota, Minneapolis, MN 55455, USA
[3] Space Sciences Laboratory, University of California, Berkeley, CA 94720, USA
[4] Department of Astrophysical and Planetary Sciences, University of Colorado, Boulder, CO 80303, USA
Received 2009 October 23; accepted 2010 January 21; published 2010 February 9

ABSTRACT

The power spectrum of density fluctuations in the solar wind is inferred by tracking small timescale changes in the electron plasma frequency during periods of strong Langmuir wave activity. *STEREO* electric field waveform data are used to produce time profiles of plasma density from which the density power spectrum is derived. The power spectra obtained by this method extend the observed frequency range by an order of magnitude while remaining consistent with previous results near a few Hertz. Density power spectral indices are found to be organized by the angle between the local magnetic field and the solar wind direction, indicating significant anisotropy in solar wind high-frequency density turbulence.

Key words: interplanetary medium – methods: data analysis – turbulence

Online-only material: color figures

1. INTRODUCTION

The solar wind at 1 AU is a good laboratory for the study of turbulent magnetized plasmas. In situ spacecraft observations of magnetic field, electric field, and density fluctuations have demonstrated a $-5/3$ power spectral index over many decades of observation frequency, often breaking into a different index above the thermal ion gyroscale (∼1 Hz fluctuations in the spacecraft frame of reference; Celnikier et al. 1987; Leamon et al. 1998; Bale et al. 2005). This spectral break is thought to be associated with the convected ion gyroradius ($k\rho_i \sim 1$) and to divide an inertial range from the shorter wavelengths where dispersion and/or dissipation become important. In the inertial range, magnetic field magnitude and density are thought to be passive scalars (Montgomery et al. 1987), their fluctuations set by and unable to influence turbulently cascading Alfvénic fluctuations driven by large-scale plasma motion close to the Sun. Below the ion gyroscale, a dispersion range is reached where single fluid theory no longer applies and ion kinetic effects become important. Beyond the dispersion range is the dissipation range where kinetic processes allow the dissipation of electric field, magnetic field, and density fluctuations through interactions with solar wind particles. Several theoretical treatments of dispersion/dissipation scale physics have been published (Schekochihin et al. 2009, Section 8.2), but few observations are available to distinguish between competing ideas. Observations of density and electric field turbulence have reached 16 Hz (Celnikier et al. 1987) and 10 Hz (Bale et al. 2005), respectively, accessing the beginning of the dispersion range. Magnetic field turbulence observations have recently been extended to ∼200 Hz using the Cluster spacecraft, directly accessing the dispersion and dissipation scales (Sahraoui et al. 2009). However, simultaneous observations of electric field, density, and magnetic field fluctuations will likely be required to definitively distinguish between formulations of magnetized plasma turbulence (Schekochihin et al. 2009).

Measurements of high-frequency (>1 Hz) density fluctuations can be used to evaluate models of plasma turbulence which predict the relative importance of compressive MHD modes in magnetized plasmas (Montgomery et al. 1987; Goldreich & Sridhar 1995). One such model is the Goldreich–Sridhar (GS) model of Alfvénic turbulence (Goldreich & Sridhar 1995). The GS model invokes a turbulent cascade in perpendicular wavenumber $k_\perp$, the condition $k_\perp \gg k_{||}$, and the concept of "critical balance" (Goldreich & Sridhar 1995). Critical balance says that the turbulent eddy turnover time is approximately equal to the Alfvén wave period $\omega \sim k_{||} v_A \sim k_\perp v_\perp$. Taken together, these conditions imply that $k_{||} \sim k_\perp^{2/3}$ and that "dissipative" scales in the perpendicular wavenumber are still far below the ion cyclotron resonance in $k_{||}$. Therefore, energy is dissipated in the perpendicular direction long before it reaches $k_{||} \sim \Omega_{ci}/v_A$. This model introduces problems for the interpretation of resonant ion cyclotron heating of heavy ions in the inner heliosphere (Cranmer et al. 1999; Leamon et al. 1999). The resonant heating models require large $k_{||}$, which in turn suggests compressive wave power.

The anisotropy of the turbulent cascade rate and turbulent fluctuation power with respect to the ambient magnetic field in solar wind plasma is a subject of much recent theoretical debate. At scales larger than the ion gyroscale, significant anisotropy has been observed in both power spectral index and fluctuation power of magnetic turbulence (Dasso et al. 2005; Horbury et al. 2008; Podesta 2009). Yet other authors find weak or no evidence of anisotropy in turbulent fluctuations (Sari & Valley 1976; Celnikier et al. 1987; Tessein et al. 2009). It is important to resolve this observational discrepancy as the presence and form of turbulent anisotropy is a key testable prediction of several contending turbulence theories (Goldreich & Sridhar 1995; Boldyrev 2005; Schekochihin et al. 2009).

In the current work, we infer in situ plasma density in 1 AU solar wind plasma at frequencies between 7 Hz and 152 Hz using a technique which involves tracking fluctuations of Langmuir wave frequency ($f_L = \omega_L/2\pi$) during periods of strong Langmuir wave activity. The Langmuir wave frequency is closely related to the electron plasma frequency ($f_p = \omega_p/2\pi$) by the Langmuir dispersion relation ($\omega_L^2 = \omega_p^2 + 3v_{th}^2 k_L^2$) for electron thermal velocity v_{th} and Langmuir wavenumber k_L. Changes in f_L primarily reflect changes in f_p, which is directly

related to plasma electron density by $n_e = (2\pi f_p)^2 m_e e_0/q_e^2$, where m_e, e_0, and q_e are the electron mass, permittivity of free space, and the electron charge, respectively.

Doppler shift and ponderomotive effects, along with variation in solar wind speed (v_{sw}), electron temperature (T_e), electron beam speed (v_b), and the angle between the local magnetic field and solar wind direction (θ_{Bv}) influence the otherwise direct relationship between plasma density and Langmuir wave frequency. In Appendix A, we show that these effects minimally impact the capability to measure high-frequency density fluctuations using Langmuir waves.

In Section 2, we present observations of Langmuir wave captures made by the *STEREO* spacecraft. We also present the inferred density profiles and density power spectra. In Section 3, we compare properties of the density power spectra data set with predictions from established turbulence models. In Section 4, we summarize our conclusions. An appendix is included to carefully address the data analysis used to infer density profiles from Langmuir wave observations. The designations parallel ($\parallel$) and perpendicular ($\perp$) are defined with respect to the local magnetic field throughout this paper.

2. OBSERVATIONS

Density fluctuation power spectra are derived from solar wind Langmuir wave observations made by the *STEREO* spacecraft, *STEREO* ahead (*STA*) and behind (*STB*). These twin spacecrafts orbit ahead of and behind the Earth at a radial distance from the Sun of 1 AU. Each spacecraft employs three 6 m, mutually orthogonal, non-biased stacer antennas which feed several experiments on board (Bale et al. 2008). The most relevant to this study is the time domain sampler (TDS) which records 130 ms bursts of voltage data at 125 kilo-samples per second, resulting in 16,384 electric field samples per capture, fast enough to observe oscillations up to 64 kHz. The TDS has a nearly flat gain response between 5 kHz and 50 kHz, while signals outside this range need to be gain corrected. Further details on the *STEREO* mission can be found in Kaiser et al. (2008) and Bougeret et al. (2008).

We study 1180 of the approximately 2500 Langmuir wave bursts recorded by *STA*/TDS and *STB*/TDS between 2006 November and 2007 February. The recorded wave bursts are identified as Langmuir waves if the *STEREO*-measured plasma frequency (f_p) determined by density measurements from the 3DP instrument on the nearby WIND spacecraft (Lin et al. 1995) match within 1 kHz for each burst. Selected bursts must also show Langmuir wave activity the entire 130 ms of the burst, and the wave power must not fall below 10^{-4} of the peak wave power measured in the burst, excluding bursts with isolated wave packets from this analysis. We impose the above criteria to ensure that the plasma frequency is well measured throughout each burst and, consequently, frequency components of the density profile down to 7.7 Hz can be resolved.

While distinguishing the source of the observed Langmuir waves is not important to this study, it should be noted that due to *STEREO*'s orbit and the lack of strong solar activity during late 2006 and early 2007, the majority of the Langmuir waves used in this study were observed as the *STEREO* spacecraft traveled through Earth's electron foreshock. However, the separation between the spacecraft and the bow shock is no smaller than 15 Earth radii for all events considered in this study. The majority of the Langmuir events considered here occur when the spacecraft and bow shock are separated by greater than 50 Earth radii.

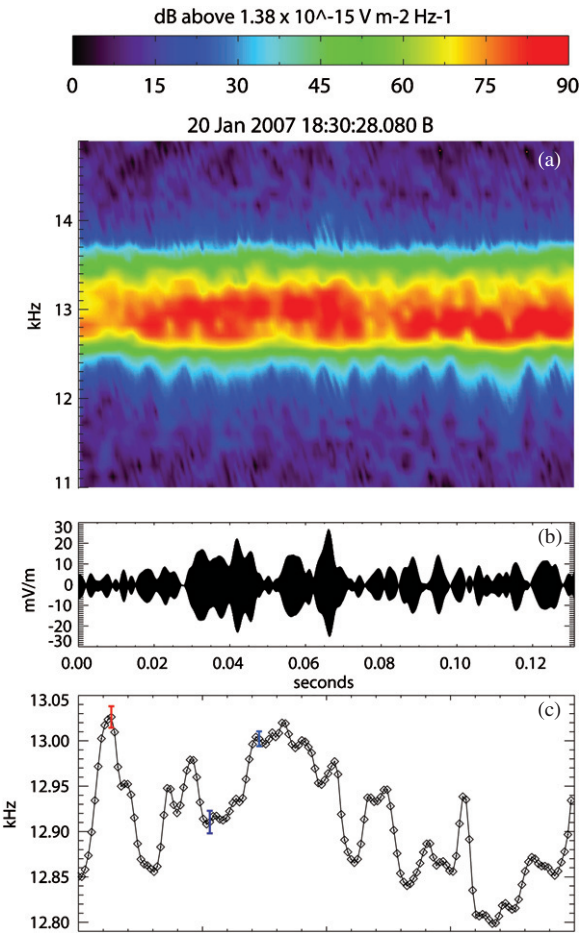

Figure 1. (a) Spectrogram of Langmuir wave in (b). (b) Langmuir waveform burst capture. (c) Peak frequency vs. time, roughly equivalent to density (see the text for details). Error bars are explained in Appendix A.

(A color version of this figure is available in the online journal.)

Interplanetary electron beams, associated with type III radio bursts, are presumed to be the other source of Langmuir wave activity.

Figure 1(b) shows a measurement of Langmuir wave electric fields. Figure 1(a) shows the associated spectrogram, and Figure 1(c) shows the derived plasma frequency profile. To generate the spectrogram, the first 8 ms (1024 data points) of the 130 ms (16,384 point) burst on each antenna is convolved with a Hanning window, then Fourier transformed and converted into a power spectrum in units of (mV^2 m^{-2} Hz^{-1}). The power spectra from each of the three antennas are then combined as $P_{\rm Total} = \sqrt{P_x^2 + P_y^2 + P_z^2}$. The 8 ms (1024 point) data window is then shifted by 10% (102 points) and a new power spectrum is taken. The process is repeated across the entire 130 ms burst. Using such a large overlap between Hanning windows limits the highest frequency in the density power spectrum which contains reliable information. The error bars in Figure 1(c) come from estimates of fluctuations in ambient plasma conditions. See Appendices A and B, respectively, for details on error bar determination and the calculation of highest reliable frequency.

Each electric field power spectral peak has a half width of 500 Hz–1 kHz and substantial fine structure near the plasma frequency. Some events show bifurcations of the plasma peak, indicating the simultaneous presence of forward and backward propagating Langmuir waves, a phenomenon variously at-

tributed to nonlinear processes including wave–wave interactions (Cairns & Melrose 1985) and Langmuir eigenmode formation (Ergun et al. 2008). This type of complex power spectral peak structure precludes the simple assignment of the observed Langmuir frequency as the power spectral maximum. Instead, a weighted average of the power spectrum is used as $f_L = \sum_n P_n f_n / \sum P_n$. This assignment produces a smoothly varying plasma frequency profile over the burst (Figure 1(c)). Given the burst duration (130 ms), the lowest density frequency resolvable is 7.7 Hz and the highest is half the sampling frequency: $\frac{1}{2}\left(0.80^{-1}\right)\ \mathrm{ms}^{-1} = 625$ Hz. Only the lower quarter of the frequencies in this range contain reliable information due to the large overlap between successive windows used to generate the frequency profile.

Because the WKB approximation does not apply at these scales (see Appendix C), fluctuations in the observed Langmuir frequency (f_L) are interpreted as directly related to fluctuations in the plasma electron density (n_e) by the relation $n_e \approx (2\pi f_L)^2 \epsilon_0 m_e / q_e^2$. Plasma environmental parameter variation and ponderomotive effects only weakly affect this relation, as discussed in detail in Appendix A.

Measured plasma density profiles contain significant power above and below the frequency band accessible by the f_L-tracking technique. Therefore, a "pre-whitening" and "post-darkening" technique is applied to the spectra to limit spectral leakage (Bieber et al. 1993; Bale et al. 2005). Briefly, this process amounts to using a power spectrum of the difference between density profile points rather than the density profile itself, then applying a compensating amplitude correction. Tests by Bieber et al. (1993) show that this procedure compensates for spectral leakage better at low frequencies. Based on their analysis, Bieber et al. (1993) determined that frequencies below $\frac{1}{3} f_{\mathrm{Nyquist}}$ show the least aliasing. These considerations restrict our maximum reliable frequency to $\frac{1}{3} f_{\mathrm{Nyquist}} = 208$ Hz. The large window overlap used to generate the density profile further restricts the maximum reliable frequency to 152 Hz. This final restriction is detailed in Appendix B.

The slope and power level of the density power spectra derived using f_L tracking matches closely in slope and spectral power with previous observations at lower frequencies (Celnikier et al. 1987). Figure 2 shows the previous measurements (by Celnikier et al. 1987) as solid lines extending down to 16 Hz. The density spectra from the current work are plotted from ∼7 Hz to ∼200 Hz. The shorter vertical lines consist of all TDS event spectra overplotted, and the heavy solid line (red online) is the average over all observations. The long vertical line shows the location of 152 Hz. The all-event averaged power level at 8 Hz matches within a factor of ∼2 the power at 8 Hz from Celnikier et al. (1987). The close alignment of observed density power spectra by two completely different observational techniques strongly indicates that f_L tracking is a sound method of measuring fine density structure. Further, it supports the assertion that variations in f_L due to T_e, v_b, and θ_{Bv} as well as ponderomotive effects only weakly affect the relation between n_e and f_L.

In this study, spectral indices derived by the Langmuir frequency tracking method are limited by counting statistics. Each spectrum results from a waveform capture with 130 ms of relatively constant amplitude Langmuir waves. When all events considered in this study (1180) are averaged together, the error on the resulting spectral index is small (±0.02). When the data are binned, each bin has a smaller number of spectra averaged together to determine the spectral index, increasing the statistical error on each power spectral index.

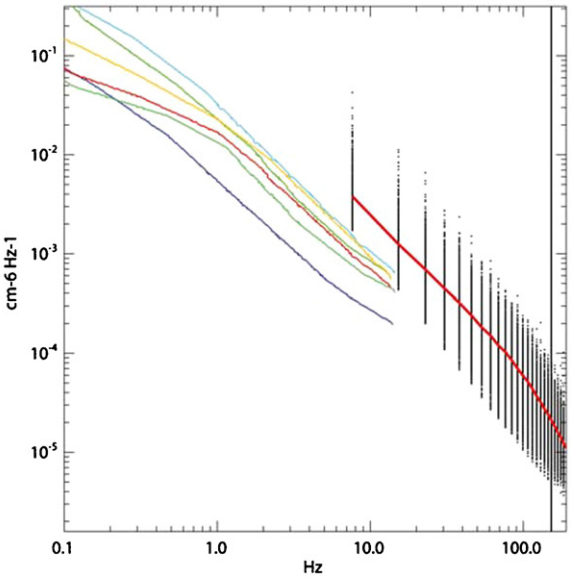

Figure 2. Solid lines below 16 Hz are density fluctuation power density vs. frequency from Celnikier et al. (1987). The vertical lines are density fluctuation power density vs. frequency from the f_L tracking method for all events overplotted. The thick solid line extending above 16 Hz is the average of all f_L tracking derived spectra.

(A color version of this figure is available in the online journal.)

3. RESULTS AND INTERPRETATION

The density power spectral index for all events averaged is -1.70 ± 0.02 for frequencies between 7.7 Hz and 152 Hz. We find that the density power spectral index depends on the angle between the solar wind velocity and the local magnetic field (θ_{Bv}). We assume that our measured fluctuations are convected by the solar wind such that the observed density fluctuation frequency is given by $\omega = \mathbf{k} \cdot \mathbf{v}_{\mathrm{sw}}$, where $\mathbf{k}$ is the wavevector of the density fluctuations. This is equivalent to assuming that the evolution timescale of the measured fluctuations is longer than the time it takes for the solar wind to convect them past the observation point such that the measured fluctuations maintain an approximately static configuration as they pass over the spacecraft. Fluctuations in density along $\mathbf{B}$ are therefore discerned when $\mathbf{v}_{sw} \parallel \mathbf{B}$. Likewise, density fluctuations perpendicular to $\mathbf{B}$ are measurable when $\mathbf{v}_{sw} \perp \mathbf{B}$. We can therefore look separately at the parallel and perpendicular wavenumber spectrum by organizing the data with respect to θ_{Bv}, the angle between $\mathbf{B}$ and $\mathbf{v}_{\mathrm{sw}}$.

Figure 3 plots the spectral index versus θ_{Bv} binned by 2° increments. Error bars are set by counting statistics such that bins averaging few spectra have large errors in determined spectral index. The straight line (red online) is a linear best fit showing the trend toward increasing spectral index with increasing θ_{Bv}. The spectral index increases from ~ -1.9 when $\theta_{Bv} \approx 0$ to ~ -1.60 when $\theta_{BV} \approx 90$.

A variation in the density power spectral index from ∼−2 to ∼−1.67 with θ_{Bv} is predicted for inertial range density turbulence by theories which invoke a critically balanced turbulent cascade (Goldreich & Sridhar 1995; Schekochihin et al. 2009). In the critically balanced case, the predicted power spectral index perpendicular to $\mathbf{B}$ is −1.67 and the anisotropic scaling $k_\parallel = k_\perp^{2/3}$ should apply such that the predicted power spectral index parallel to $\mathbf{B}$ is −2. This behavior has been observed recently by Horbury et al. (2008) and Podesta (2009) for inertial range magnetic field turbulent fluctuations.

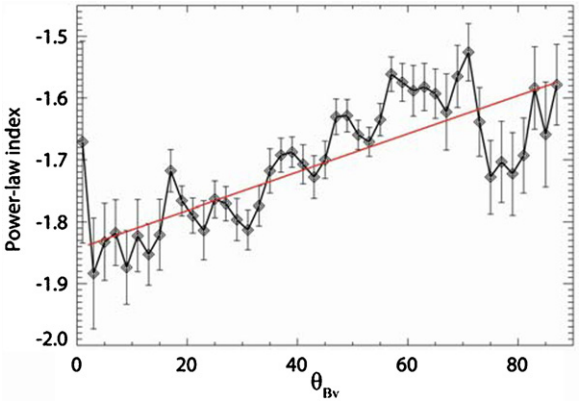

Figure 3. Density power spectral index as a function of θ_{Bv}, binned by 2°. Error bars are set by counting statistics such that bins averaging relatively few spectra have large errors in determined spectral index.

(A color version of this figure is available in the online journal.)

Other authors have attributed such anisotropy in the spectral scaling of turbulent magnetic fields in terms of coherent solar wind structure, specifically magnetic discontinuities (Sari & Valley 1976). Sari & Valley (1976) found that anisotropy in the spectral scaling of turbulent magnetic fields was not significant when periods showing coherent solar wind structures, specifically magnetic discontinuities, were removed from their data set. Sari & Valley (1976) reported between 1 and 6 magnetic discontinuities per day in their data. Given that the *STEREO* data used here sample only 130 ms with a duty cycle of 1–30 samples per day, it is unlikely that a significant fraction of *STEREO* wave captures coincide with magnetic discontinuities.

Further, the conditions used to exclude events where the plasma frequency was not well determined ensure that the data used in this study are free of events with plasma frequency (density) discontinuities. Requirements are imposed in the data selection (see Section 2) that (1) the Langmuir wave power is strong enough to discern a plasma peak throughout the event and (2) the density implied by the measured plasma peak must be, for the entire duration of the event, within 1 kHz of the plasma frequency determined by convected WIND density measurements. Therefore, we do not believe that magnetic discontinuities of the type reported in Sari & Valley (1976) or density discontinuities significantly influence the *STEREO*/TDS data used in this study.

Gyrokinetic (GK) theory is a turbulence model which assumes critically balanced anisotropic turbulence explicitly and makes testable predictions of density power spectral scaling (Schekochihin et al. 2009). Therefore, we compare our observations of dispersion range density power spectral scalings with GK predicted scalings. According to GK theory, dispersion range density and magnetic power spectra are expected to show steeper indices (−2.33 perpendicular to B) than in the inertial range (−1.66 perpendicular to B). The anisotropy of density fluctuations predicted by GK theory in the dispersion/dissipation range ($k_{||} = k_{\perp}^{1/3}$) is greater than density fluctuation anisotropy in the inertial range ($k_{||} = k_{\perp}^{2/3}$; Schekochihin et al. 2009).

Cluster observations of magnetic field turbulence reported by Sahraoui et al. (2009) are consistent with GK predictions. Specifically, Sahraoui et al. (2009) observed a magnetic spectrum with an index of ~ -1.66 in the inertial range, an index of ~ -2.33 in the dispersion range, and an index of ∼3.9 in the dissipation range. However, Sahraoui et al. (2009) do not explicitly include in their report spectral index variation with θ_{BV} during their measurements.

Figure 3 shows that the current data are inconsistent with GK theoretical predictions. While the *STEREO*/TDS density measurements are in the dissipation/dispersion range (>1 Hz in the spacecraft frame), the observed spectral anisotropy instead matches that predicted for the inertial range ($k_{||} = k_{\perp}^{2/3}$). Further, the steepest density power spectral index for $\theta_{BV} > 80°$ is ~ -1.73, much shallower than the GK prediction of −2.33. The *STEREO*/TDS data does agree with the prediction that solar wind density fluctuations are significantly anisotropic, even if that anisotropy is not as strong as predicted by GK theory.

From the measurements of Sahraoui et al. (2009) and those reported here, we conclude that solar wind density and magnetic field fluctuations do not share power spectral scaling relations below the ion gyroscale. It is therefore unlikely that density is a passive turbulent scalar below the ion gyroscale.

The observations presented here indicate that significant anisotropy in the power spectral scaling of solar wind density turbulence below the ion gyroscale exists. However, the observed scaling of power spectral indices is inconsistent with specific predictions for density turbulence below the ion gyroscale made by GK theory.

4. CONCLUSION

The authors introduced a technique to infer rapid fluctuations in plasma density using Langmuir wave observations, opening the door to observations of density turbulence at frequencies an order of magnitude above previous observations. It was argued on theoretical grounds that changes in solar wind plasma parameters on millisecond timescales only weakly perturb measurements of the density fluctuation power spectra. The density power spectra generated by this method match well with previous observations at overlapping frequencies, supporting insensitivity of this method to plasma parameter fluctuation. Trends in power spectral index demonstrate significant anisotropy of solar wind plasma density turbulence below the ion gyroscale. However, the data are at odds with specific theorized scalings of density turbulence as determined by GK turbulence models.

The authors are grateful to the entire *STEREO* team, and specifically the *STEREO*/WAVES team, for their continued efforts and support, and for access to *STEREO*/TDS data. This work was funded by NASA's *STEREO*/WAVES Phase E and an NASA Earth and Space Sciences Fellowship (09-Helio09R-0001).

APPENDIX A

RELATING f_L AND n_e

To convert between f_L and plasma density n_e, we begin with the relation $\omega_L = \omega_T + \omega_D$ where $\omega_T = \omega_p(1-3T_e/(m_e v_b^2))^{-\frac{1}{2}}$ is the theoretical Langmuir frequency using the dispersion relation for a hot, weakly magnetized plasma and the Langmuir wave resonance condition $k_L v_b = \omega_T$. We also define ($f_L = \omega_L/2\pi$). The frequency $\omega_D = k_L v_{\rm sw}\cos(\theta_{Bv})$ is due to Doppler shift as the solar wind convects the Langmuir wave past the spacecraft. For Langmuir waves, $\mathbf{k_L}$ is parallel to $\mathbf{B}$, therefore ω_D depends on θ_{Bv} and the magnitudes of $\mathbf{k_L}$ and $\mathbf{v}_{\rm sw}$. The electron temperature is T_e, and m_e, k_L, $v_{\rm sw}$, and θ_{Bv} are the electron mass, the Langmuir wavevector, the solar wind speed,

and the angle between **B** and $\mathbf{v}_{sw}$, respectively. Solving for ω_L:

$$\omega_L = \omega_p \left(1 - \frac{3T_e}{v_b^2 m_e}\right)^{-\frac{1}{2}} \left(1 + \frac{v_{sw}}{v_b}\cos(\theta_{Bv})\right). \quad \text{(A1)}$$

To determine the relationship between f_L and (n_e), it is critical to determine what effects variable T_e, v_b, and θ_{Bv} have on the relationship between ω_L and ω_p.

Variation of T_e and v_b must be estimated by physical argument since there are no observations of electron distribution functions at cadences approaching 1 ms. To isolate variable T_e and v_b, we assume briefly that $\cos(\theta_{Bv}) = 0$. Using A1: $d\omega_L/\omega_p = -\frac{1}{2}\gamma\,(dT_e/T_e)$ and $d\omega_L/\omega_p = \gamma\,(dv_b/v_b)$, where $\gamma = (3T_e/me)(1 - 3T_e/(m_e v_b^2)^{-\frac{3}{2}}$. For common solar wind parameters at 1 AU (1 eV $< T_e <$ 50 eV, and $6v_{th} < v_b$), γ is less than 1, therefore variation in T_e and v_b alters $d\omega_L/\omega_p$ only weakly.

Further, variation in T_e over 1 ms should be negligible because the distance a 10 eV solar wind electron travels in 1 ms at 1 AU (∼1.33 km) is greater than the scale size of millisecond plasma density fluctuations (∼400 m). Therefore, the thermal part of the local electron distribution describes electrons from a volume which is large compared to the measured density fluctuation scale, implying that the electron temperature is stable on millisecond and longer timescales.

The electron beam speed v_b may evolve by dispersion or quasilinear flattening as the beam propagates past the location of the Langmuir waves, but these variations are likely small on timescales of 130 ms. For Langmuir waves to grow, the condition $\omega_T = v_b k_L$ must be satisfied for at least one Langmuir growth time (≈0.5–1 s). During this time, $d\omega_T/\omega_T$ must not change more than 3% to obtain a typical observed f_L peak width of 1 kHz/30 kHz. Therefore, dv_b/v_b must also vary by <3% over 0.5–1 s. This amounts to $dv_b/v_b < 0.01\%$ per millisecond given a linearly changing v_b. The 3% constraint on f_L width is an upper bound since most of the f_L width is from Doppler broadening, and the true resonance width is much smaller than 3%.

Assuming now that v_b and T_e are nearly constant and again using Equation (A1): $d\omega_L/\omega_p = (1 - 3T_e/v_b^2 m_e)^{-\frac{1}{2}}\,(v_{sw}/v_b)\cos(\theta_{Bv})\,(d\cos(\theta_{Bv})/\cos(\theta_{Bv}))$. For typical 1 AU solar wind parameters ($T_e = 10$ eV, $v_b = 5v_{th}$, $v_{sw} = 400$ km s^{-1}), and a worst case $\theta_{Bv} = 0$, $d\omega_L/\omega_p = 0.0304\,d\cos(\theta_{Bv})/\cos(\theta_{Bv})$. Again, variation in θ_{Bv} causes small variation in f_L. Additionally, the maximum θ_{Bv} variation over 1 ms is <2°, determined by extrapolating a measured magnetic fluctuation power spectrum (Alexandrova et al. 2008) to 1 kHz and assuming $B = 9$ nT. Unlike T_e and v_b, θ_{Bv} varies with **B**, which is itself a turbulent quantity. Therefore, when θ_{Bv} is small, n_e and **B** are weakly coupled in the observed frequency profile. Likewise, when θ_{Bv} is large, the Doppler shift is small and the turbulent properties of f_L are those of n_e.

To further demonstrate that millisecond timescale fluctuations in v_b, v_{sw}, and θ_{Bv} do not strongly influence the results of this paper, we compute error bars on the frequency profile in Figure 1. For this calculation, we assume typical solar wind environmental values of $v_{sw} = 400$ km s^{-1}, $T_e = 10$ eV, $v_b = 0.08\,c$, and $\theta_{Bv} = 45°$. As argued above, the variation in v_b is likely to be <3%, and the variation in θ_{Bv} likely less than 2° (4.5%). Variation in the solar wind speed on these timescales has never been measured, but we adopt a very conservative estimate of 5% maximum fluctuation over 1 ms. The error bars on the computed frequency peaks are show in Figure 1. Left to right, the error bars represent $5\%v_{sw}$, $3\%v_b$, and $4.5\%\theta_{BV}$ fluctuations, respectively.

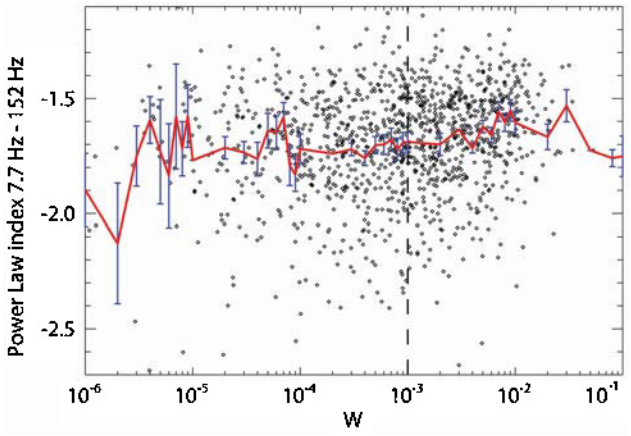

Figure 4. Density spectral index as a function of $W = \epsilon_0 E^2/(2\,n\,k_B\,T_e)$. The solid line shows spectral index binned by $\log_{10}(W) = 0.1$.
(A color version of this figure is available in the online journal.)

It is also known that Langmuir waves of sufficient amplitude can modify the local plasma density by the ponderomotive force. For the ponderomotive effect to be negligible, a typically cited criterion is that the ratio of the wave energy to the kinetic energy of the surrounding plasma should be small: $W = \epsilon_0 E^2/(2\,n\,k_B\,T_e) < 1 \times 10^{-3}$. Using the mean electric field strength in each TDS data burst, $W < 1 \times 10^{-3}$ for all events used in this study. However, some electric field peaks of short duration (∼10 ms) have high enough amplitude to push W above 1×10^{-3}, though values of W such that $W > 1 \times 10^{-2}$ are rare in this study. Figure 4 shows a scatter plot of density power spectral index, derived using frequencies from 7.7 Hz to 152 Hz, as a function of the maximum W in each Langmuir waveform. There is a slight increase in power spectral index from −1.72 to −1.62 between $W = 1 \times 10^{-3}$ and $W = 1 \times 10^{-2}$. However, this variation is within the estimated error on spectral index and is not evident for any other range of W. Additionally, the trend presented in Figure 3 is independent of whether only events with $W < 1 \times 10^{-3}$ or events with $W > 1 \times 10^{-3}$ are used. Finally, qualitative comparison of $W > 1 \times 10^{-3}$ structures and density profiles shows that $W > 1 \times 10^{-3}$ structures are not consistently associated with density decreases. Therefore, density power indices derived from Langmuir wave packets containing structures with W between 1×10^{-3} and 1×10^{-2} are only weakly influenced by ponderomotive effects.

APPENDIX B

WINDOW OVERLAP EFFECTS

The large overlap between windows used to generate each density profile serves to smooth the resultant profile, but also causes adjacent density points to become strongly correlated. Density profile points which are larger distances apart are progressively less correlated. The strongly correlated points correspond to high frequencies in the resultant density power spectrum and therefore an accurate spectrum excludes the appropriate high frequencies. To quantify where the exclusion should begin, we specify a few parameters.

First, we are using 1024 point Hanning windows and sliding them by 10% to obtain each successive density profile point. This means that adjacent windows share 90% of their electric field time series data points. A metric of the correlation between spectral estimates made by successive overlapping windows

Table 1
Overlap Correlation Between Successive Windows Shifted by $N\,\tau$ and the Frequency Needed to Resolve Spectral Power for Fluctuations at those Scales

$N\,\tau$	Overlap with 0 τ (r)	OC	$f_{\rm Nyquist}$ (Hz)
1	90	94	610
2	80	77	304
3	70	55	203
4	60	33	152
5	50	17	122

(referred to as the overlap correlation, OC) was determined by Harris (1978). When OC = 100, the spectra derived using the data under two adjacent windows are entirely correlated. When OC = 0, no artificial correlation is added to the data by window overlap.

$$\mathrm{OC}(r) = \frac{\sum_{j=0}^{rN-1} \omega_j \omega_{j+(1-r)N}}{\sum_{j=0}^{N-1} \omega_j^2}. \quad \text{(B1)}$$

Here, j is an index which counts the data points, N is the total number of data points per window (1024 in this case), r is the fractional overlap (0.9 here), and ω_j is the value of the window-convolved data at point j.

For the specific case of a Hanning window with 90% overlap between windows, the OC for two adjacent windows, corresponding to two adjacent density profile points, is 94. In the *STEREO*/TDS data treated in this paper, adjacent windows are separated by 102 E-field points (8.1×10^{-4} s). We define this number as 1τ. The frequency required to resolve fluctuations from density profile points separated by 1τ is therefore ~610 Hz. Based on these considerations, we construct Table 1.

We select 152 Hz (points 4τ apart) as the upper bound of reliable frequencies in the density power spectrum because it is the first frequency where the OC is significantly less than 50. At frequencies below 152 Hz the OC decreases further, increasing the reliability of the density power spectrum data at low frequencies.

After considering the effects of window overlap in detail, it should be noted that for density power spectral frequency cutoffs of 203 Hz, 152 Hz, and 122 Hz the primary results of this paper remain valid. The averaged density power spectrum matches closely with the results of Celnikier et al. (1987) and the spectral index increases with θ_{Bv} from ~1.90 to ~1.60.

APPENDIX C

WKB

The group velocity of a Langmuir wave resonant with a 10 $v_{\rm th}$ electron beam (considering 10 eV thermal electrons) is $\approx$ 360 km s^{-1}, which is of the same order as the solar wind velocity. Therefore, Langmuir waves observed during each 130 ms event are actively propagating across solar wind density structures and WKB effects may be important.

Under the WKB approximation, the frequency of a propagating Langmuir wave stays constant as the wave traverses density gradients. The wavevector ($\mathbf{k_L}$) changes to stay resonant with the electron beam driving the Langmuir waves. The profiles presented in this paper show Langmuir frequency varying as a function of time, contradicting WKB predictions in the limit that the Langmuir frequency fluctuations are weakly affected by changes in the resonant electron beam or significant variation in magnetic connectivity to the electron beam source during each 130 ms observation (see Appendix A). Frequency variation due to density structure is expected because for the scales studied here, the WKB approximation is not valid.

The WKB approximation is valid as long as change wavelength of a Langmuir wave is small compared to one wavelength. From this definition, Kellogg et al. (1999) derived an expression for WKB validity:

$$\left(\frac{\pi}{3}\right)\left(\frac{\omega}{ck_L}\right)^3\left(\frac{c^2}{v_{th}^2}\right)\left(\frac{c}{\omega_{pe}}\right)\left(\frac{1}{nv_{\rm sw}}\right)\left(\frac{dn}{dt}\right) \ll 1. \quad \text{(C1)}$$

Defining the left-hand side of the above equation as ϵ, we solve the above equation using typical solar wind parameters ($v_{\rm sw}$ = 400 km s^{-1}, T_e = 10 eV, n = 9 cm^{-3}) and $dn/n \approx 0.0016$ per millisecond, which correspond to density fluctuations of the order observed in Figure 1. For weak foreshock electron beams ($\omega/k_Lc \approx v_b/c \approx 6v_t$), we find $\epsilon \approx 0.01$. For moderate foreshock electron beams ($v_b/c \approx 10v_t$), we find $\epsilon \approx 0.1$. For solar electron beams, $v_b/c \approx 1/3$, we find $\epsilon \approx 1$. The $\epsilon \ll 1$ condition is marginally valid for weak foreshock electron beams. Changing solar wind parameters do not strongly alter these results and electron beam speeds are typically greater than $6v_{th}$ for solar wind Langmuir waves. Therefore, we conclude that the WKB approximation does not hold for frequency (or density) fluctuations on the observed rapid timescales.

REFERENCES

Alexandrova, O., Carbone, V., Veltri, P., & Sorriso-Valvo, L. 2008, ApJ, 674, 1153
Bale, S. D., Kellogg, P. J., Mozer, F. S., Horbury, T. S., & Reme, H. 2005, Phys. Rev. Lett., 94, 215002
Bale, S. D., et al. 2008, Space Sci. Rev., 136, 529
Bieber, J. W., Chen, J., Matthaeus, W. H., Smith, C. W., & Pomerantz, M. A. 1993, J. Geophys. Res., 98, 3585
Boldyrev, S. 2005, ApJ, 626, L37
Bougeret, J. L., et al. 2008, Space Sci. Rev., 136, 487
Cairns, I. H., & Melrose, D. B. 1985, J. Geophys. Res., 90, 6637
Celnikier, L. M., Muschietti, L., & Goldman, M. V. 1987, A&A, 181, 138
Cranmer, S. R., Field, G. B., & Kohl, J. L. 1999, Space Sci. Rev., 87, 149
Dasso, S., Milano, L. J., Matthaeus, W. H., & Smith, C. W. 2005, ApJ, 635, 181
Ergun, R. E., et al. 2008, Phys. Rev. Lett., 101, 051101
Goldreich, P., & Sridhar, S. 1995, ApJ, 438, 763
Harris, F. J. 1978, Proc. IEEE, 66, 51
Horbury, T. S., Forman, M., & Oughton, S. 2008, Phys. Rev. Lett., 101, 175005
Kaiser, M. L., Kucera, T. A., Davila, J. M., St.-Cyr, O. C., Guhathakurta, M., & Christian, E. 2008, Space Sci. Rev., 136, 5
Kellogg, P. J., Goetz, K., Monson, S. J., & Bale, S. D. 1999, J. Geophys. Res., 104, 17069
Leamon, R. J., Smith, C. W., Charles, W., Ness, N. F., Matthaeus, W. H., & Wong, H. K. 1998, J. Geophys. Res., 103, 4775
Leamon, R. J., Smith, C. W., Charles, W., Ness, N. F., & Wong, H. K. 1999, J. Geophys. Res., 104, 22331
Lin, R. P., et al. 1995, in The Global Geospace Mission, ed. C. T. Russel (Dordrecht: Kluwer), 125
Montgomery, D., Brown, M. R., & Matthaeus, W. H. 1987, J. Geophys. Res., 92, 282
Podesta, J. J. 2009, ApJ, 698, 986
Sahraoui, F., Goldstein, M. L., Robert, P., & Khotyaintsev, Y. V. 2009, Phys. Rev. Lett., 102, 231102
Sari, J. W., & Valley, G. C. 1976, J. Geophys. Res., 81, 5489
Schekochihin, A.A, Cowley, S. C., Dorland, W., Hammett, G. W., Howes, G. G., Quataert, E., & Tatsuno, T. 2009, ApJS, 182, 310
Tessein, J. A., Smith, C. W., MacBride, B. T., Matthaeus, W. H., Forman, M. A., & Borovsky, J. E. 2009, ApJ, 692, 684